PHYSICAL REVIEW E **67**, 010303(R) (2003)

Self-similar dynamic quasi-two-dimensional sand fronts

J.-F. Boudet, S. Gauthier, Y. Amarouchene, and H. Kellay
Centre de Physique Moléculaire Optique et Hertzienne (UMR 5798), Université Bordeaux I, 351 cours de la Libération, 33405 Talence Cedex, France

(Received 22 October 2002; published 22 January 2003)

We report on a study of advancing quasi-two-dimensional sand fronts on an inclined flat and thin strip confined between two vertical plates. These fronts form when a thin initial stream of sand running down the flat obstacle gets trapped at some distance from the injection point. Right after this trapping, the front starts to advance upstream and grow in time. The shapes at successive times are found to be self-similar in time. The stability conditions for the obtained fronts are also outlined. A simple model for interface dynamics gives reasonable predictions for the observed shapes.

DOI: 10.1103/PhysRevE.67.010303 PACS number(s): 45.70.Mg, 45.70.Qj, 47.54.+r

Granular materials can give rise to a variety of patterns such as sand dunes and sand ripples, which are subjects of considerable attention [1–3]. Some field studies have provided quantitative information on the shapes of certain types of dunes [4] which permits some comparisons with theoretical models [5]. From the fundamental point of view, understanding the dynamics, shapes, and interfacial properties of large assemblies of beads or grains, such as sand dunes, sand ripples, and sand fronts is a difficult and timely problem [6–9]. Granular materials exhibit behavior that crosses the frontiers between different states of matter and pose fundamental problems in statistical physics, nonlinear dynamics, and mechanics [10,11].

To simplify the study of dynamic sand piles, we have used a quasi-two-dimensional geometry, in which ''sand fronts'' are produced by simply pouring a jet of sand down an inclined thin and flat plane. This experiment allows the generation of dynamic and advancing sand fronts with curved self-similar shapes. The self-similar shape of the front turns out to be well described by a simple model for the interface: a driven convection-diffusion equation. It is important to note here that desert dunes do not show self-similarity as is the case here. This maybe related either to differences due to dimensionality or to the absence of other length scales in our problem.

The experimental apparatus (Fig. 1) consists of a quasi-two-dimensional cell composed of two transparent and flat plates held vertically and separated by a distance b of either 1 cm or 2 cm, and two flat and thin inclined planes A and B which are sandwiched between the two vertical plates. The granular material used is either sieved dry beach sand, which is relatively polydisperse and whose grains are irregular (mean diameter is 0.3 mm), or glass beads, which are relatively monodisperse and whose grains are spherical (mean diameter is 0.45 mm). A jet of sand is first poured from a funnel on the first plane A. This first plane guides the running sand, in the form of a thin and dilute stream, before encountering the second plane that has an inclination angle θ with the horizontal. The range of angles extends from a few degrees to slightly less than the angle of repose of the material used on the substrate. The running thin stream of sand on the second plane ends up getting trapped at some distance R_i from the injection point. Friction acts to decelerate the movement of the particles down the inclined plane which come to a stop at R_i. This is confirmed by measuring the time evolution of the front of the stream of sand running down the inclined plane. Once the sand gets trapped further downstream, a small pile forms giving rise to a sand front growing upstream as it is constantly fed with the incoming flux of sand (see Fig. 2).

In this experiment, the main control parameter is the inclination angle θ of the second plane. The mass flux per unit time Q was kept constant in a single experiment but was varied to check for its importance. The results concern the distance of trapping R_i from the injection point and the profile $h(x,t)$ of the propagating front along with its temporal evolution. The initial trapping is displayed in Fig. 2(a) and the evolution at different times after the initial trapping instant is shown in Figs. 2(b) and 2(c). Note that in Figs. 2(b,c), there are no or very few grains which go behind the propagating front. All the grains are trapped and are only used to construct the advancing dynamic sand front. Two parts [Fig. 2(d)] characterize a typical structure: a large static and compact zone (dark in the images) and a relatively fuzzy part where the grains are in motion especially near the front; this is seen through the presence of the streaks from individual particles. Note that their length and, therefore, the

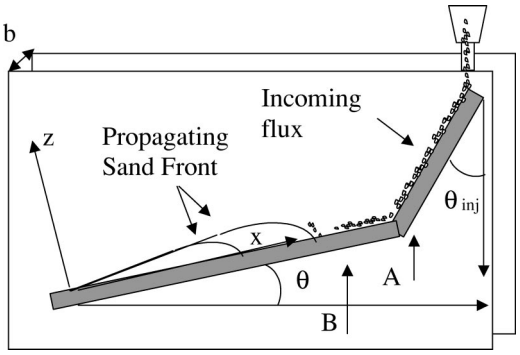

FIG. 1. Setup: two plexiglass plates separated by a distance b of either 1 cm or 2 cm, two inclined planes A and B sandwiched between the two plates, and a funnel for sand injection. The first plane A, fixed at an angle θ_{inj}, laminarizes the flow and sets the initial velocity of the stream. The second plane is fixed at a variable angle θ.

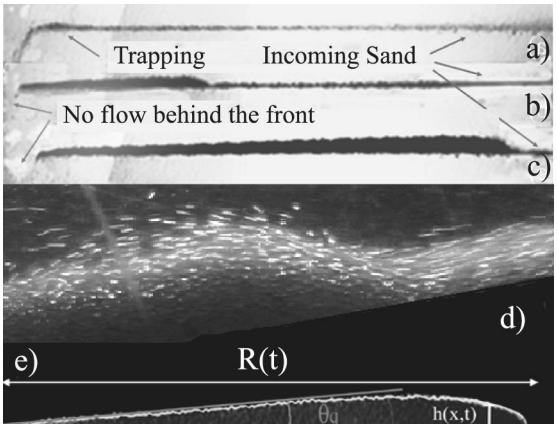

FIG. 2. (a) Initial trapping, (b) and (c) the growth of the sand front ($\theta=20°$), (d) the region near the front showing the initial stream and the flow of particles (camera shutter speed: 1/500 s, $\theta=12°$), (e) a typical sand front and the different parameters.

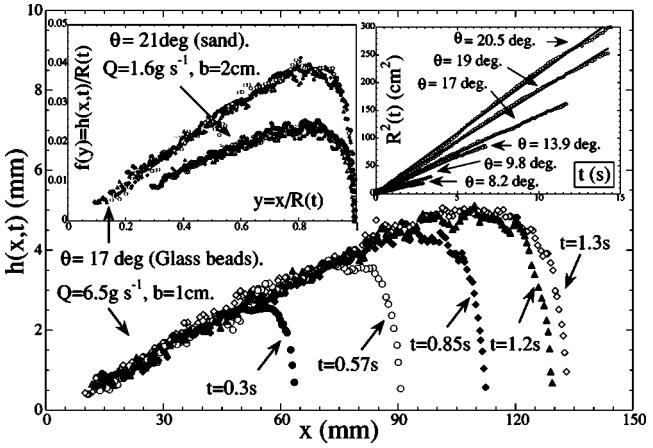

FIG. 3. Several profiles obtained at different times. Left inset: The same profiles rescaled by the base length of the structure $R(t)$; a second set of profiles obtained for sand at an angle of 21° at successive times of 2.8 s, 4.6 s, 6.1 s, 8.8 s, and 10.7 s is also shown. Right inset: variation of the length $R^2(t)$ versus time using sand.

velocity of the particles decreases as they climb up over the front and proceed to the tail region. These moving particles originating from the initial stream manage to go over the top of the structure and even beyond [Fig. 2(d)] to make it grow vertically as well as horizontally. As no grains go beyond the trapping point, the particles must decelerate and stop before reaching this point. These are the main mechanisms for the construction of the propagating sand front. The curvature at the front of the structure relaxes once the injection is stopped. The tail of the structure [Fig. 2(e)] is roughly linear and has a small well-defined angle θ_q with the inclined plane. This angle is found to be between 1° and 8° depending on the material used, the injection flux Q, and the angle θ. When the front grows, this angle stays roughly constant with time.

Our central result concerns the successive propagating sand fronts at different times after the initial trapping instant. The fronts are self-similar as they grow both parallel and perpendicular to the inclined plane. Their shapes are independent of time once the horizontal and vertical axes are rescaled by the base of the pattern $R(t)$. In Fig. 3, the profiles of propagating sand fronts from the same experiment photographed at different times are displayed; in the inset to this figure the same profiles rescaled by their respective lengths are shown. The self-similarity is striking. Both the characteristic length and the characteristic height of the structure grow similarly in time. Mass conservation dictates that both these scales, the maximum height and the length of the structure should scale as $\sqrt{t}$ which is verified experimentally (see inset to Fig. 3, where the dependence $R^2=Dt$, where D has dimensions of a diffusion constant, is clearly seen). The range of times for which self-similarity can be determined is about a factor of 5 between the initial time and the final time, while the angles θ for which self-similarity is easily seen extend from 8° to 22°. Smaller angles were more difficult to analyze mainly because the injection region is reached relatively quickly.

Let us now discuss the properties of the trapping length R_i and the angle θ_q. In Fig. 4(a), the variation of R_i as a function of θ is plotted for different values of θ_{inj} and Q. As θ increases, the trapping occurs further downstream. The increase of R_i versus θ is intuitive; gravity plays a more important role when θ is large. The variation of R_i versus θ turns out to be well described by invoking the friction of the granular material on the plate. By following the movement of the initial front of the running stream of sand as it decelerates down the incline and before it comes to rest, we determined that the trapping distance R_i is determined by the balance between friction and gravity. This balance gives $R_i=V_0^2/2(\mu\cos\theta-\sin\theta)g$, where μ is the dynamic friction coefficient between the sand and the inclined plane and which turns out to be independent of the velocity within the accuracy of our measurements; θ is the angle and g is gravity. V_0 is the initial velocity of the front of the stream. This form fits the data very well as can be seen in Fig. 4. The friction coefficient turns out to be about 0.46 for the glass beads and between 0.5 and 0.6 for the sand.

Figure 5(a) shows that the angle θ_q is very small and decreases linearly with increasing θ, with a small slope that

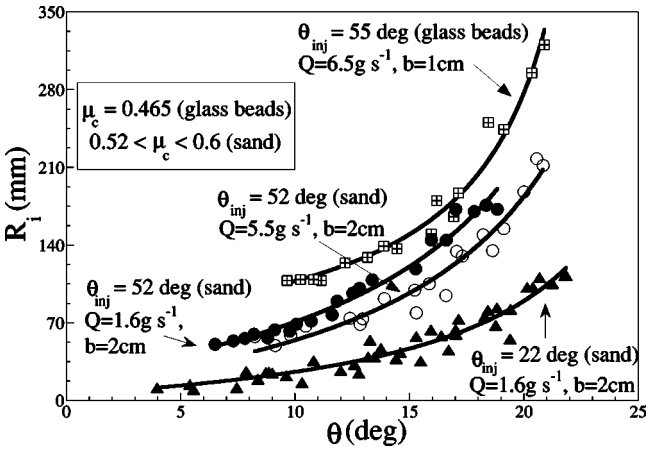

FIG. 4. The trapping length R_i versus θ, solid lines are fits using the expression in the text.

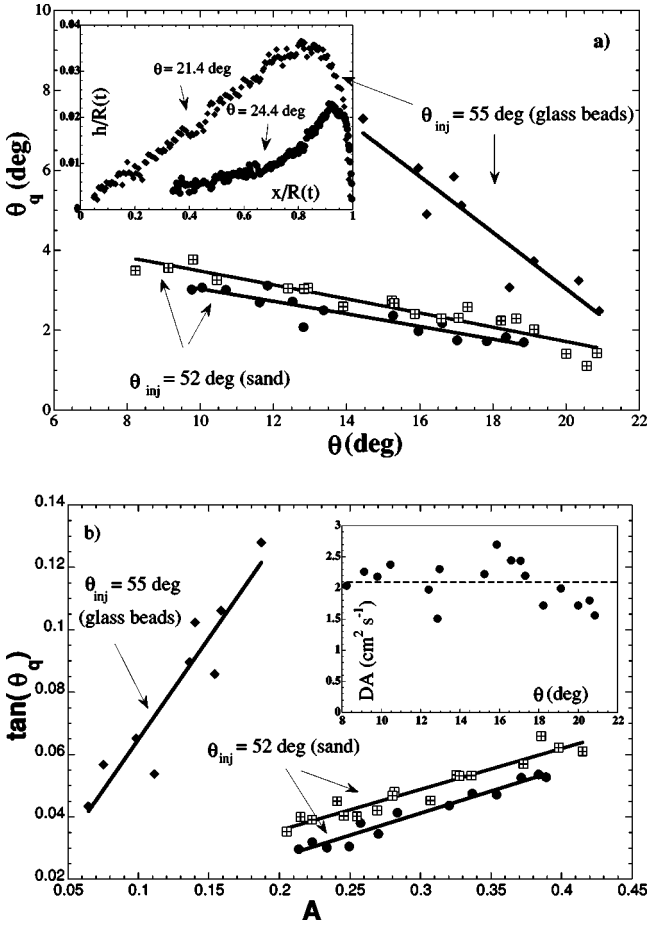

FIG. 5. (a) The angle θ_q versus the angle of the obstacle θ for the same conditions as in Fig. 4. The granular material used is either beach sand or glass beads. Inset: profiles for θ smaller than the critical angle θ_l and larger but very close to θ_l, which is estimated at 24°. (b) The same data as in (a), for $\tan(\theta_q)$ versus the reduced acceleration A. Inset: DA versus the angle θ.

seems to depend on the material used. The angle of this zone with the horizontal axis (i.e., $\theta_q+\theta$) grows with θ and stays smaller than θ_C, the static critical angle of repose of the sand used. In light of the roughly linear dependence of θ_q versus θ, θ_q goes to zero at a specific angle θ_l, which is not very different from θ_C but seems to depend on the injection flux and the angle θ_{inj} (this angle fixes the initial velocity V_0 of the stream of sand). The angles θ_l and θ_c for the displayed data are 24 and 27, respectively, for the glass beads and 30 and 36 for the sand. From direct tests, when θ is greater than θ_l, the trapping is much less efficient, and the front does not form unless triggered by blocking the sand near the outlet of the cell. If triggered, the sand front can form but is not stable and disappears eventually. Slightly above θ_l, a front can form spontaneously and advance upstream but its shape is very different. The tail is long, and relatively flat with a small height, while the front is narrow and shows up as a bump as can be seen in the inset of Fig. 5(a). Close inspection of the tail part of the unstable structures such as the one shown in the inset of Fig. 5(a) shows that the grains are in motion and rolling down the incline.

The dependence of $\tan(\theta_q)$ versus the angle of the plate θ turns out to be similar to that of the aspect ratio H/R of the maximum height of the ripple to that of its base length. This dependence is determined solely by the factor $A=(\mu\cos\theta-\sin\theta)$ (a reduced acceleration) as both quantities are linear versus A. As can be seen in Fig. 5(b), $\tan(\theta_q)$ follows this law very well. This dependence gives a natural explanation for the limiting angle θ_l as it turns out to be fixed by the dynamic friction coefficient μ (we find 0.45 for the glass beads and 0.57 for the sand from θ_l, values not very different from those determined above). Basically, above this angle, gravity is stronger than the friction force maintaining the structure in place. The mechanism behind the above relation is a simple energy balance. In order for the flow of grains to reach the top of the front and make it grow vertically, their kinetic energy has to balance their potential energy as they climb up the structure. The ratio of kinetic to potential energy is given by $1/2V^2/gH$; considering that the average velocity of the stream of particles as they approach the base of the front is given by $V^2/2=AgR$ (due simply to a balance of gravity and friction on the bottom plate; we checked the variation of the velocity of the stream and its dependence on the length and the angle directly), this energy ratio is then AR/H which is constant in a single experiment and independent of Q giving H/R and, therefore, $\tan(\theta_q)$ (approximately) proportional to A as confirmed by the measurements. In addition, this constant energy ratio seems to determine the vertical growth rate of the sand front. Setting the vertical growth rate (RdH/dt) as simply proportional to the product of this energy ratio by the total growth rate $(dS/dt=Q/\rho_c b)$, the constant D can be calculated. This gives D proportional to $Q/A\rho_c b$ [and therefore inversely proportional to $\tan(\theta_q)$ which is intuitive], where ρ_c is the density of the sand which is not far from its compact value. The dependence of D on A is borne out experimentally as seen in the inset of Fig. 5(b). While the aspect ratio decreases as the angle θ approaches θ_l, the coefficient D increases.

The above considerations clarify most of the properties of the propagating sand front notably their aspect ratio and their propagation speed in relation to the interplay between gravity and friction against the bottom plate. A crucial issue, however, concerns the understanding of the shape or profile $h(x,t)$ of the obtained sand fronts which displays a linear tail and a curved front. For our purposes, we use a simple model that was shown, recently, to work reasonably well for stationary dynamic dunes [12]. The model, which is close in spirit to the model proposed by Hwa and Kardar in the early 1990s [6], postulates a driven convection-diffusion equation for the profile of the propagating sand front with no distinction between moving and static parts within the pile as is done in more recent models [8]. This driven convection-diffusion equation can be written as: $(\partial h/\partial t)+[\partial(v_x h)/\partial x]-D'(\partial^2 h/\partial x^2)=q(x,t)$. In these equations, $v_x(x,t)$ is a mean convection velocity along the x axis. D' is a diffusion constant and $q(x,t)$ is a velocity perpendicular to the x axis due to the injection of the sand upstream and fixed by conservation of the mass flux. Due to the self-similarity, we have made the following simplifications [using the reduced variable $y=x/R(t)$]; $v_x(x,t)=v(t)y$ and $q(x,t)$

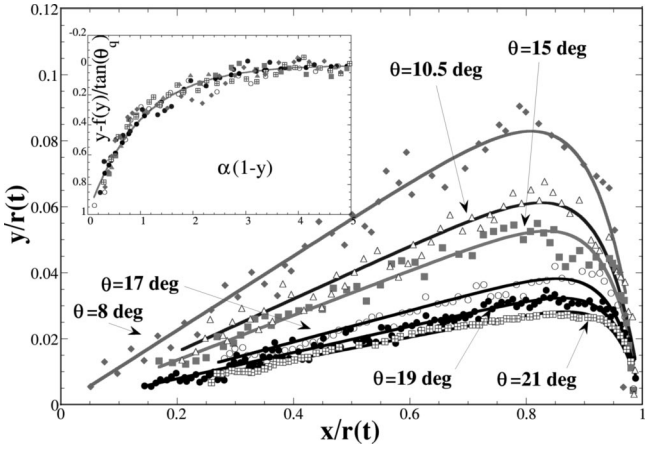

FIG. 6. Different profiles for different angles θ. The lines are fits using the expression in the text. Inset: Collapse of profiles for different angles onto a universal curve. The solid line is the theoretical prediction.

$=2v(t)\tan(\theta_q)y$ [where $v(t)=dR(t)/dt=D/2R(t)$]. If we use the property $h(x,t)=R(t)f(y)$, we obtain a new equation for $f(y)$. The linear dependence of q on $\tan(\theta_q)y$ is consistent with mass conservation. The functional form of v_x can be found directly from the self-similarity of the profiles. The resulting equation for f can be solved exactly: one obtains an exact solution $f(y)=\tan(\theta_q)[y-\sinh(\alpha y)/\sinh(\alpha)]$, where $\alpha=\sqrt{D/D'}$. The structure of this solution is simple: a superposition of a linear solution with slope $\tan(\theta_q)$ and a term originating from the diffusive term in the equation giving the curvature at the front. This solution is a very good approximation to the profiles of the advancing sand fronts obtained for different angles θ (see Fig. 6). The fits were carried using one free parameter α. Since D is known, D' turns out to be roughly constant with a value of about 0.021 cm^2/s. As is apparent here, the shapes depend on two related parameters, namely, $\tan(\theta_q)$ and α which both depend on the angle θ. In order to collapse all of these profiles versus the angle, one needs to take the variation of both these parameters versus θ into account. This is done in the inset of Fig. 6, where we plot $[y-f(y)/\tan(\theta_q)]$ versus $\alpha(1-y)$ (to put the front at position 0) giving simply the $\sinh(\alpha y)/\sinh(\alpha)$ dependence that is displayed as the solid line. The agreement with this form is excellent for structures obtained with different inclinations.

More rigorous theoretical analyses on sand fronts use a more recent model introduced to describe the interface of a pile of sand as well as the dynamics of avalanches [8,9] (see Ref. [7] for earlier attempts). These so-called ''BCRE equations'' are a sophistication of earlier ''single variable'' models which describe the interface of a pile of sand as governed by a diffusion process that relaxes possible surface roughness [6]. These models are powerful in giving the dynamics of avalanches as an example and treat the dynamic piles as composed of a static and a moving part using appropriate couplings between the two. Recently, in a theoretical work [9], based on a formalism introduced in Ref. [8], in the case of a granular flow near a boundary, self-similarity was suggested for the advancing sand fronts. However, their findings differ from ours: the similarity solution found was in x/t while the similarity observed here is in $x/\sqrt{t}$. It must be noted here that these models make use of parameters (convection velocity, diffusion coefficients, etc.) which are assumed to be constant. In addition, the presence of a granular external flux was not considered in Ref. [9]. It may well be that the use of appropriate parameters with the correct dependence on temporal and spatial coordinates in these models may describe our results in more detail than the model we use, but this is beyond the scope of this paper.

The advancing sand fronts obtained in our simple experiment are self-similar and present profiles which are understandable on the basis of a simple driven convection-diffusion equation for the interface. Such results, although relevant to a quasi-two-dimensional geometry, may shed some light on the dynamics of sand dunes and sand ripples which are a source of both fascination and awe.

[1] R.A. Bagnold, *The Physics of Blown Sand and Desert Dunes* (Chapman and Hall, London, 1941).

[2] K. Pye and H. Tsoar, *Aeolian Sand and Sand Dunes* (Unwin Hyman, London, 1990).

[3] N. Lancaster, *Geomorphology of Desert Dunes* (Routledge & Kegan Paul, London, 1995).

[4] G. Sauermann, P. Rognon, A. Poliakov, and H.J. Hermann, Geomorphology **36**, 47 (2000).

[5] G. Sauermann, K. Kroy, and H.J. Hermann, Phys. Rev. E **64**, 031305 (2001).

[6] T. Hwa and M. Kardar, Phys. Rev. Lett. **62**, 1813 (1989); Phys. Rev. A **45**, 7002 (1992).

[7] A. Mehta, J.M. Luck, and R.J. Needs, Phys. Rev. E **53**, 92 (1996); A. Mehta, R.J. Needs, and S. Dattagupta, J. Stat. Phys. **68**, 1131 (1992).

[8] J.P. Bouchaud *et al.*, J. Phys. I **4**, 1383 (1994); Phys. Rev. Lett. **74**, 1982 (1995).

[9] L. Mahadevan and Y. Pomeau, Europhys. Lett. **46**, 595 (1999).

[10] S.R. Nagel, Rev. Mod. Phys. **64**, 321 (1992); M. Jaeger, S.R. Nagel, and R.P. Behringer, *ibid.* **68**, 1259 (1999); J. Duran, *Sables, Poudres, et Grains* (Eyrolles Sciences, Paris, 1997); P.-G. de Gennes, Rev. Mod. Phys. **71**, S374 (1999); L.P. Kadanoff, *ibid.* **71**, 435 (1999).

[11] *Powders and Grains 97*, edited by R.P. Behringer and J.T. Jenkins (Balkema, Rotterdam, 1997).

[12] Y. Amarouchene, J.F. Boudet, and H. Kellay, Phys. Rev. Lett. **86**, 4286 (2001).